Robust Array Configuration for a Microwave Interferometric Radiometer: Application to the GeoSTAR Project

F. Torres, A. B. Tanner, S. T. Brown, and B. H. Lambrigsten

***Abstract*—The Geostationary Synthetic Thinned Array Radiometer represents a promising new approach to microwave atmospheric sounding from geostationary orbit based on passive interferometry. One of the major concerns about the feasibility of this new concept is related to the ability of the sensor to cope with the failure of one or several of its single receivers/antennas. This letter shows that the inclusion of a small percentage of additional antennas significantly reduces the degradation of radiometric resolution caused by such receiver failure. Impact of antenna failure is analyzed, taking into account two test images with very different spatial harmonic content. A tradeoff analysis of several array topologies is performed so as to minimize the number of additional antennas while keeping worst case radiometric error within a reasonable level.**

***Index Terms*—Interferometry, radiometry, redundancy remote sensing.**

I. Introduction

GEOSTATIONARY microwave sounders were not feasible up to now due to the large aperture required to achieve the sufficient spatial resolution. In this sense, the Geostationary Synthetic Thinned Array Radiometer (GeoSTAR) represents a promising new approach to microwave atmospheric sounding from geostationary orbit based on passive interferometry [1]. This instrument may complement future infrared sounders and enable all-weather temperature and humidity soundings and rain mapping. While low-Earth orbit satellites provide coverage in relative narrow swaths, with a revisit time of 12–24 h, a geostationary Earth-orbit (GEO) satellite can provide continuous hemispheric or regional coverage, making it possible to monitor highly dynamic phenomena such as hurricanes.

GeoSTAR was proposed as a solution to Geostationary Operational Environmental Satellite Systems microwave sounders, in response to the 2002 National Aeronautics and Space Administration (NASA) research announcement calling for proposals to develop new technologies. Sponsored by the NASA Instrument Incubator Program, the Jet Propulsion Laboratory is currently developing a proof-of-concept ground-based demonstrator operating with four 100-MHz channels between 50 and 54 GHz, which has already produced very encouraging results [2].

The assessment on system performance degradation due to antenna takes into account the particular GeoSTAR configuration (staggered Y) [2] and basic properties of GEO images. It follows the systematic methodology described in [3], which shows that antenna failure mainly impacts on radiometric accuracy (systematic spatial rms error in the image) due to the degradation of the secondary lobes of the synthesized beam. On the other hand, since the noise-equivalent Delta T (NEDT) (radiometric sensitivity or noise-equivalent temperature resolution caused by finite correlation time in the estimation of the visibility samples) and the spatial resolution (half-power beamwidth of the synthesized beam) are marginally affected by a single antenna failure [3], they will not be taken into account in this letter. The objective of this letter is to identify the optimum array topology in an early stage of the project in order to set the basis for a comprehensive robustness analysis, as described in [3].

II. GeoSTAR Configuration

GeoSTAR consists of a thinned array of 300 receiving elements deployed in a "Y" configuration. The complex cross correlation between the signals collected by any pair of antennas yields one sample of the so-called visibility function, which is the measure of a particular spatial harmonic. The "Y" shape distribution of the antennas give the visibility samples over a hexagonal grid, which minimizes the number of required elements to cover the spatial domain u-v (antenna separation measured in wavelengths). In an ideal case, the visibility function is the Fourier transform of the brightness temperature given in the direction cosine coordinate system.

Fig. 1 shows an example of the antenna arrangement for the GeoSTAR configuration with a number of elements per arm Nel $= 8$. Note that the three arm axes meet in an equilateral triangle, not a point, unlike other Y arrays (e.g., the configuration adopted in the Soil Moisture and Ocean Salinity mission [4]). The three arms are plotted in different symbols to highlight that the only cross correlations measured by the instrument correspond to those baselines formed by antenna

Manuscript received May 11, 2006; revised July 14, 2006. This work was performed in the frame of the GeoSTAR project, funded by the National Aeronautics and Space Administration, during F. Torres sabbatical stage at the California Institute of Technology, Jet Propulsion Laboratory (Grant PR2005-0427, Spanish Ministry of Education and Science).

F. Torres is with the Department of Signal Theory and Communications, Polytechnic University of Catalonia, 08030 Barcelona, Spain (e-mail: xtorres@tsc.upc.edu).

A. B. Tanner, S. T. Brown, and B. H. Lambrigsten are with Jet Propulsion Laboratory, California Institute of Technology, Pasadena, CA 91109 USA.

Color versions of one or more of the figures in this paper are available online at http://ieeexplore.ieee.org.

Digital Object Identifier 10.1109/LGRS.2006.886427

1545-598X/$25.00 © 2007 IEEE

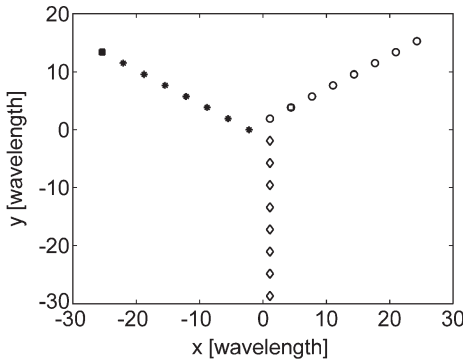

Fig. 1. GeoSTAR staggered-Y antenna configuration for eight elements per arm: ◇ arm #1, * arm #2, and ○ arm #3. The squares (□) represent the position of two possible antenna failures: Antenna 8 in arm #2 and antenna 2 in arm #3.

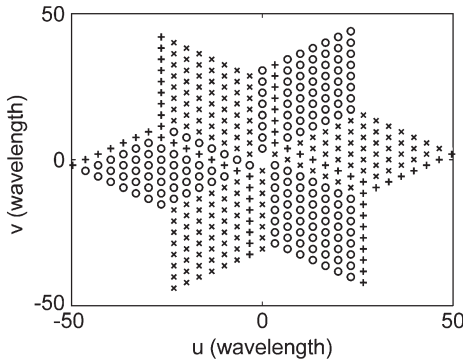

Fig. 2. GeoSTAR coverage in the u-v domain for eight elements per arm. Nominal visibilities $(\times)$, conjugate visibilities $(\circ)$, and $(+)$ represent the (u, v) visibility samples lost due to the two antenna failures given in Fig. 1.

pairs within different arms. This constraint is imposed by the demodulation process currently foreseen for this instrument [2], although it does not represent a loss of coverage in the sampling u-v domain. The instrument measures the cross correlations for all antenna pairs arranged according to the following arm combinations: arm #2 versus arm #1, arm #3 versus arm #2, and arm #1 versus arm #3. These correlations give the so-called nominal visibilities in the (u, v) plane, marked with crosses $(\times)$ in Fig. 2. Taking into account that the visibility is a Hermitian function, the visibility samples corresponding to the $(-u, -v)$ positions, marked with circles $(\circ)$ in Fig. 2, are directly computed as the conjugate of the nominal measurements. As an example, Fig. 2 also shows the set of visibility samples that would be lost—plus sign $(+)$—in case that antennas marked with a square $(\square)$ in Fig. 1 are in failure. The field of view (FOV) is given by the elemental antenna spacing, which is set to 3.75 wavelengths in order to match the Earth disk when viewed from GEO (17.5°). This is also the elemental antenna pattern half-power beamwidth. A comprehensive description of GeoSTARs main characteristics can be found in [2].

III. Test Images

In order to assess the impact of antenna failure, we have selected two images that present a quite different brightness-temperature distribution within the Earth's contour. Both images show the Earth and sky brightness temperature, as seen

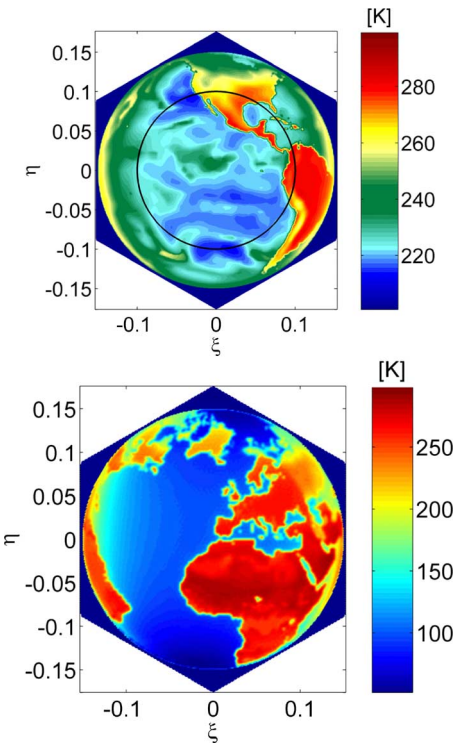

Fig. 3. (Top) Pacific and (bottom) Atlantic images retrieved by an ideal instrument with 100 antennas per arm. The simulation uses standard rectangular Fourier techniques over hexagonally sampled signals [4]. Elemental antenna separation is 3.75 wavelengths, which sets the FOV to match the Earth's contour. The effect of sky alias has been removed.

from a geostationary orbit, in the direction cosine domain ($\xi = \sin\theta\cos\varphi, \eta = \sin\theta\sin\varphi$). They are given in a 1500×1500 rectangular grid, which allows a maximum spatial resolution of 48 km at boresight. The first image corresponds to AMSU-A 50.3-GHz channel over the Pacific. This image presents a smooth temperature distribution within the Earth's contour. Its mean brightness temperature is 226 K, and its standard deviation is $\sigma_{\mathrm{TB}} = 16$ K. The original data have been obtained from National Centers for Environmental Prediction (NCEP) Reanalysis fields [5] given in a $2.5^\circ \times 2.5^\circ$ grid over a $0.25^\circ \times 0.25^\circ$ land mask (spatial resolution at a boresight of 280 and 27 km, respectively), which yield a low but significant harmonic content in the 50-km spectrum range. In order to have an image with larger harmonic content and contrast, a second case consisting of a fake image from the brightness temperature of sea and land at 2.4 GHz has been selected. Its mean temperature is 170 K, and its standard deviation is $\sigma_{\mathrm{TB}} = 83$ K. The original data are given in a $1^\circ \times 1^\circ$ grid over a $1/12^\circ \times 1/12^\circ$ land mask (spatial resolution at a boresight of 110 and 27 km, respectively), as done in [6]. Truncation and finite coverage of the imaging process gives a difference in relation to the original image of $\sigma_{\Delta T} = 0.5$ K for the Pacific image and $\sigma_{\Delta T} = 1.41$ K for the Atlantic image, the latter mainly concentrated around the land–sea transitions. The statistics are computed in the circle established by the 45° incidence angle within the Earth's contour ($r < 0.1$ in Fig. 3, top). In order to perform the simulations, first, the theoretical visibility samples are computed by a direct fast Fourier transform (FFT) over a hexagonal grid [7], considering an instrument with $\mathrm{Nel} = 100$ antennas per arm. Antenna

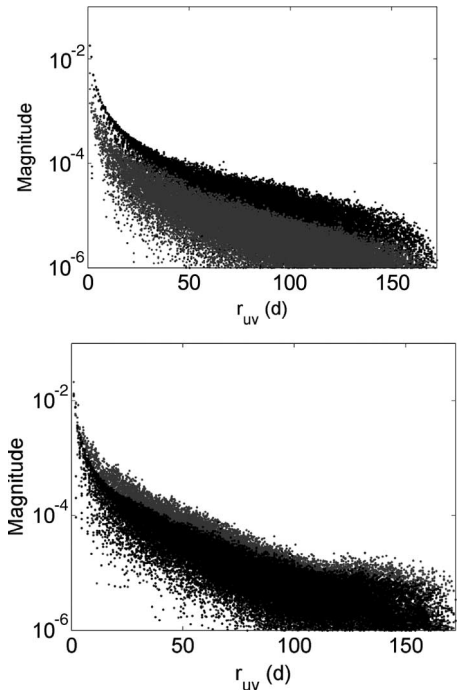

Fig. 4. Magnitude of the contrast visibility $V_{\rm ctr}$ (gray) and the reference visibility $V_{\rm ref}$ (black), normalized to $T_{\rm sys} = 600$ K, for (top) the Pacific and (bottom) Atlantic images as a function of distance to the u-v plane center r_{uv}.

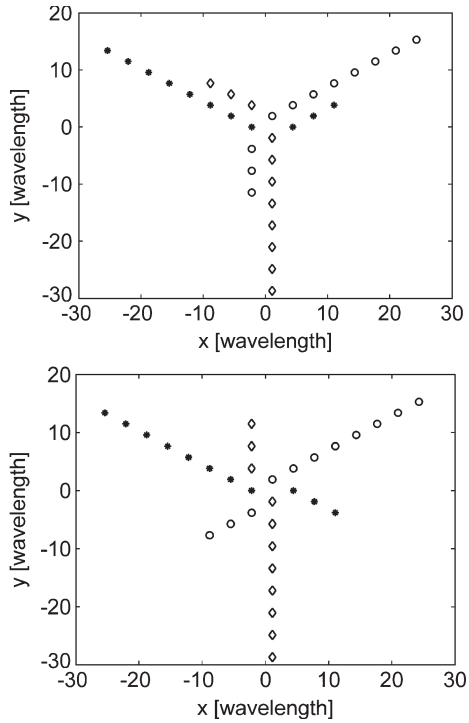

Fig. 5. GeoSTAR optimum redundant topologies for $\mathrm{Nel} = 8$ and two redundant antennas per arm. Antennas with the same symbol are assigned to the same arm so as to form antenna pairs and compute correlations.

separation is $d = 3.825\lambda$, which gives an unambiguous FOV that encloses the Earth's diameter, as seen from GEO ($\sim 17.5^\circ$), and a spatial resolution at a boresight better than 50 km. Then, an inverse FFT is applied to retrieve an estimate of the original image in a hexagonal cell (Fig. 3).

At this point, it is worth to mention that traditional methods used in radioastronomy to deal with incomplete sampling of the u-v space, such as CLEAN or maximum entropy method (MEM), are very suited to deal with quasi-point sources filling an empty FOV, such as a cluster of stars. They also make use of the positive nature of the image to be restored. In [6], it is shown that the CLEAN method is not suited to deal with extended sources of radiation such as the Earth brightness temperature (this also applies to the MEM). Camps *et al.* [6] also describe the method to use the *a priori* information: the brightness-temperature map in the direction cosine domain can be split into two well-defined contributions $T = T_{\rm ctr} + T_{\rm ref}$. The first term is the temperature contrast $T_{\rm ctr}$ that represents a zero-mean image where the sky is at 0 K and the Earth disk is at the temperature deviation from its mean value. The second term is the reference temperature $T_{\rm ref}$ that corresponds with an image where the Earth disk is at its constant mean temperature and the sky at a known temperature distribution. Since a single antenna failure has a small effect on the estimated Earth mean temperature, this one can be estimated, in a first iteration, by zero padding the missing samples in V and retrieving T. The visibility samples are related to the temperature distribution as $V = G \cdot T$, where G is a linear operator (e.g., the FFT in an ideal interferometer). Therefore, measured visibilities can be split into $V = V_{\rm ref} + V_{\rm ctr}$. This arrangement is important because the information of the image is contained exclusively by the contrast term $V_{\rm ctr}$. In case that a visibility sample is missing, the term $V_{\rm ref}$ can be estimated theoretically from the temperature distribution $T_{\rm ref}$. In fact, the inversion procedure is performed to retrieve the contrast temperature as

$$\begin{aligned} T_{\rm ctr} &= G^{-1} V_{\rm ctr} \\ &= G^{-1}(V - V_{\rm ref}). \end{aligned} \tag{1}$$

This procedure eliminates the contribution from sky alias in the retrieved image as well as the ringing effect close to the sharp Earth–sky transition, which is caused by the truncation of the visibility spectrum to the star shape in the u-v domain (Fig. 2). Additionally, it improves the stability of the inversion procedure in case that a Fourier transform cannot be used [6], [7]. Fig. 4 shows the harmonic content of the contrast visibility $V_{\rm ctr}$ normalized to $T_{\rm sys} = 600$ K, as a function of the distance to the center of the (u, v) plane. As shown, both the Pacific and Atlantic images present a large percentage of energy concentrated in the shorter spatial harmonics. The harmonic content of the normalized reference image $V_{\rm ref}$ is also shown for comparison.

IV. Radiometric Error in Failure Mode

This section is devoted to analyze the effect of failure of one antenna/receiver, which causes the loss of all correlations related to it. The following assumptions are taken into account.

1) A receiver fails or works perfectly. Partial failure is not taken into account. Receiver failure is identified from

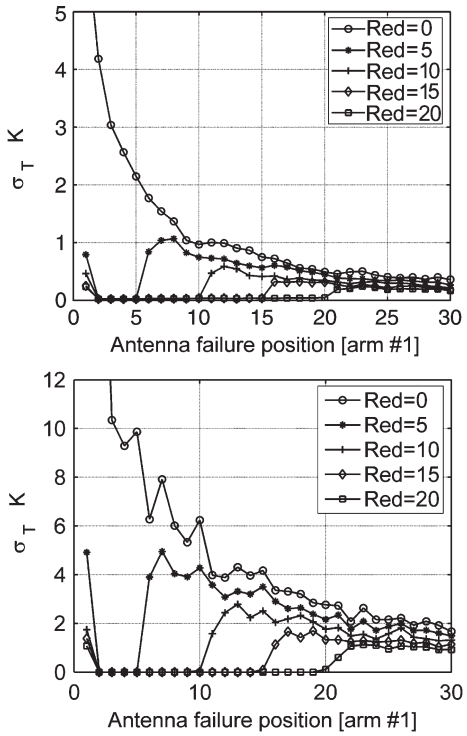

Fig. 6. Radiometric error due to a single antenna failure. Absolute error is related to the image temperature dispersion: (top) $\sigma_{\rm TB} = 6.9$ K for the Pacific image and (bottom) $\sigma_{\rm TB} = 83$ K for the Atlantic image.

the induced artifacts in the image, anomalous detected signals, or by any other means.

2) Since the information of the reference image $V_{\rm ref}$ is retrieved theoretically, only the information relating to the contrast brightness temperature $T_{\rm ctr}$ is lost. The missing sample is zero padded.

If the same (u, v) visibility sample is measured by different antenna pairs, the so-called redundant baselines, failure of one antenna has a minimum impact in system performance since there is no loss of the (u, v) coverage. Full redundancy can only be achieved by doubling the array. However, redundancy of the shorter baselines significantly reduces the degradation of radiometric resolution caused by such receiver failure due to the fact that a large percentage of the energy in the image is concentrated in the lower harmonics (Fig. 4).

Fig. 5 shows two examples of topologies used to implement redundancy of such shorter baselines. The two configurations present the same redundant (u, v) coverage, which is slightly better than several small variations that have also been analyzed. The topology in Fig. 5 (top) is the one selected because of mechanical considerations.

Antenna failure causes a systematic distortion on the retrieved image, which depends on the number and position of antenna failures [3]. Fig. 6 shows the radiometric error caused by a single antenna failure as a function of its distance to the center of the array. A different number of redundant antennas per arm (red $= 0$, 5, 10, 15, and 20) are taken into account. The radiometric error is computed as the rms difference of the retrieved image in the failure mode from the retrieved image by an ideal instrument (Fig. 2). The error is computed inside the Earth's contour in the area delimited by the 45° incidence angle ($r < 0.1$ in the direction cosine domain).

TABLE I
WORST CASE RADIOMETRIC ERROR DUE TO SINGLE FAILURE

Relative radiometric error $\sigma_{\Delta T} / \sigma_{TB}$				
Redundancy	*Red=5*	*Red=10*	*Red=15*	*Red=20*
Pacific image	6.7%	3.6%	2.0%	1.5%
Atlantic image	6.9%	3.9%	2.3%	1.7%

[1] Worst-case occurs when single failure takes place within a set of approximately 10% of all antennas.

As shown in Fig. 6, when redundancy is not taken into account $(\circ)$, the loss of a receiver close to the center of the array produces catastrophic effects on the retrieved image. As the failure occurs in antennas more distant from the array center, its impact is much lower. Therefore, the inclusion of a small set of redundant antennas close to the array center highly reduces the impact of a single antenna failure. The absolute error $\sigma_{\Delta T}$ in both the Atlantic and Pacific images is quite different. However, when compared to the dispersion in the original contrast image $\sigma_{\rm TB}$, the relative error is similar (Table I). It has been verified that, for small errors, radiometric error due to multiple antenna failure adds quadratically.

V. CONCLUSION

This letter has analyzed the impact of antenna failure on radiometric performance of the interferometer, which is one of the major concerns in this kind of sensors. It has been shown that failure of one antenna close to the center of the array produces large errors in the retrieved temperature map. However, since the energy of the image is mainly concentrated in the shorter baselines, adding additional antennas in the array, so as to partially recover the missing measurements, can largely mitigate the effect of the failure. Several array configurations used to arrange these additional antennas have been analyzed, which must be arranged in a "Y" shape in order to have the same properties of the main array. Due to the particular GeoSTAR demodulating scheme [2], the two configurations shown in Fig. 5 are the optimum in terms of redundant coverage (response to antenna failure).

The image can be decomposed into two contributions. The first one consists of the Earth disk at its mean temperature and the sky also at a known temperature. In this case, the associated visibility samples can be estimated theoretically. The second contribution corresponds to the temperature deviation from the mean within the Earth disc. Since this mean temperature can be well retrieved, even in the case that a few antennas are in failure, only the information relating temperature dispersion within the Earth disk is lost in case of failure. The missing visibility samples are zeroed in order to perform the image retrieval algorithm.

Two images with very different statistical properties have been analyzed to show that the relative error due to a single antenna failure is similar when compared to the image temperature dispersion. That is, the impact of antenna failure is

more related to the sampling geometry than to the harmonic content of the images. This comes from the fact that the system only measures a small set of short baselines, which are the ones with higher energy content, and makes them critical in case of failure. In both images, the worst case error can be reduced to a small percentage of the scene rms temperature distribution by adding about 15%–20% of additional antennas. If redundancy is included, a single failure of most of the antennas in the array produces zero or almost negligible impact in system performance, whereas the worst case error is related to a single failure within a small set of antennas (about 10%) in the whole array.

ACKNOWLEDGMENT

The authors would like to thank the Polytechnic University of Catalonia (Spanish Research and EU Feder project TEC2005-06863-C02-01/TCM, "Técnicas interferométricas, polarimétricas y biestáticas para sistemas de teledetección por microondas) for the simulations based on the simulator InRadSim, which has been adapted to the GeoSTAR configuration.

REFERENCES

[1] B. Lambrigtsen, W. Wilson, A. Tanner, T. Gaier, C. Ruf, and J. Piepmeier, "GeoSTAR—A microwave sounder for geostationary satellites," in *Proc. IGARSS*, 2004, vol. 2, pp. 777–780.

[2] A. B. Tanner, S. T. Brown, S. J. Dinardo, T. M. Gaier, P. P. Kangaslahti, B. H. Lambrigtsen, W. J. Wilson, J. R. Piepmeier, C. S. Ruf, S. M. Gross, B. H. Lim, S. Musko, and S. Rogacki, "Initial results of the GeoSTAR Prototype," in *Proc. IEEE Aerosp. Conf.*, Big Sky, MT, Mar. 4–11, 2006, p. 9.

[3] M. Vall-llossera, N. Duffo, A. Camps, I. Corbella, F. Torres, and J. Bara, "Reliability analysis in aperture synthesis interferometric radiometers: Application to L-band Microwave Imaging Radiometer with Aperture Synthesis instrument," *Radio Sci.*, vol. 36, no. 1, pp. 107–117, Jan. 2001.

[4] E. Kalnay *et al.*, "The NCEP/NCAR 40-year reanalysis project," *Bull. Amer. Meteorol. Soc.*, vol. 77, no. 3, pp. 437–471, 1996.

[5] Y. Kerr, J. Font, P. Waldteufel, and M. Berger, (2000)."The second of ESA's Opportunity Missions: The Soil Moisture and Ocean Salinity Mission—SMOS,"*ESA Earth Obs. Q.*, vol. 66, 18f. [Online]. Available: http://www.esrin.esa.it/export/esaLP/SEMHONZ990E_LPsmos_0.html

[6] A. Camps, J. Bará, F. Torres, and I. Corbella, "Extension of the CLEAN technique to the microwave imaging of continuous thermal sources by means of aperture synthesis radiometers," *J. Electromagn. Waves Appl.*, vol. 12, no. 3, pp. 311–313, 1998.

[7] A. Camps, J. Bara, I. Corbella, and F. Torres, "The processing of hexagonally sampled signals with standard rectangular techniques: Application to 2-D large aperture synthesis interferometric radiometers," *IEEE Trans. Geosci. Remote Sens.*, vol. 35, no. 1, pp. 183–190, Jan. 1997.